

Article

Decreasing Electrical Resistivity of Ag Film by Low-Temperature Evaporation and Sintering through Azeotrope Application

Sang Hoon Jung¹, Jae Eun Park¹ and Jong-Hyun Lee^{1,2,*} 

¹ Department of Materials Science and Engineering, Seoul National University of Science and Technology, Seoul 139-743, Republic of Korea

² Research Institute for Future Convergence Materials, Seoul National University of Science and Technology, Seoul 139-743, Republic of Korea

* Correspondence: pljh@snut.ac.kr

Abstract: In the temperature-sensitive components, such as perovskite solar cells, large-area electrical connections with high electrical conductivity are also required. To fulfill the requirements, low-temperature evaporation was realized by preparing binder-free pastes with Ag flakes and a solvent mixture, followed by sintering at 140 °C. The mixed solvent was based on viscous α -terpineol with the addition of an appropriate amount of dipropylene glycol methyl ether acetate or diethylene glycol diethyl ether to achieve an azeotrope composition, followed by the addition of a low-molecular-weight hydroxypropyl cellulose to increase the viscosity and thixotropy. During sintering at 140 °C in air for up to 30 min, the paste with 49.5 wt% α -terpineol, 49.5 wt% dipropylene glycol monomethyl ether acetate, and 1 wt% hydroxypropyl cellulose mixture exhibited an excellent electrical conductivity of $7.72 \times 10^{-6} \Omega \cdot \text{cm}$ despite the implementation of low-temperature sintering. The excellent processability of the prepared Ag-based pastes at 140 °C demonstrated their potential for novel application areas.

Keywords: binder-free Ag paste; viscous solvent; hydroxypropyl cellulose; azeotrope composition; electrical resistivity; low-temperature evaporation; sintering



Citation: Jung, S.H.; Park, J.E.; Lee, J.-H. Decreasing Electrical Resistivity of Ag Film by Low-Temperature Evaporation and Sintering through Azeotrope Application. *Metals* **2024**, *14*, 1123. <https://doi.org/10.3390/met14101123>

Academic Editor: Nebojša Nikolić

Received: 12 August 2024

Revised: 27 September 2024

Accepted: 29 September 2024

Published: 2 October 2024



Copyright: © 2024 by the authors. Licensee MDPI, Basel, Switzerland. This article is an open access article distributed under the terms and conditions of the Creative Commons Attribution (CC BY) license (<https://creativecommons.org/licenses/by/4.0/>).

1. Introduction

Perovskite solar cells are actively being developed as window-type solar cells owing to their advantages of translucency and color generation [1–13]. Transparent electrode materials with excellent transparency and electrical conductivity should be developed to fabricate high-efficiency window-type perovskite solar cells. A representative example is pattern printing using a Ag particle-based paste, which has excellent oxidation resistance and sinterability [14–18]. However, the efficiency of perovskite materials can decrease when heat-treated at temperatures of 100 °C. As such, electrode materials and printing processes that provide high conductivity and light transmittance at low process temperatures are required [18]. For pastes containing resin, including low-temperature curing resins, such as polydimethylsiloxane (silicone), acrylic, or phenoxy, excellent electrical conductivity is difficult to achieve owing to the formation of percolation networks by contact between Ag particles [19–23]. For example, Fang et al. developed a hybrid silver paste by adding micro- and nano-sized Ag fillers into epoxy and organic vehicles for application in thermally sensitive flexible electronics. They reported an electrical resistivity of $8.1 \times 10^{-5} \Omega \cdot \text{cm}$ after sintering at 150 °C for 30 min [24]. In contrast, for resin-free formulations with lower appropriate viscosity, only Ag particles remain with the evaporation of viscous solvents, facilitating sintering between the particles and achieving excellent electrical conductivity [25–31]. For example, Liu et al. mixed spherical and flake silver particles and obtained an electrical resistivity of $3.31 \times 10^{-5} \Omega \cdot \text{cm}$ after sintering at 200 °C for 45 min [25]. Also, Zhao et al. presented superior electrical conductivity characteristics,

reporting a resistivity of $1.08 \times 10^{-5} \Omega\text{-cm}$ after sintering micron-sized silver particles at 140°C for 30 min [26].

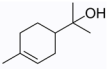
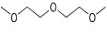
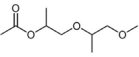
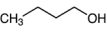
In this study, a low-temperature sintering paste was prepared by mixing Ag particles with a mixture of solvents, which can be removed at 140°C by evaporation, and a thickener. Flake-shaped Ag microparticles were used as fillers; however, they are less sinterable than nanoparticles, which are more cost-effective and provide better uniform mixing, making them easier to manufacture into a paste. The mixing ratio of the viscous solvents and thickeners, which was considered the main factors for improving the electrical conductivity by enhanced sinterability, was optimized by measuring the electrical resistivity and microstructure of the formed film with different ratios. The electrical conductivity of the film formed in this resin-free paste was directly affected by the sintering degree between the Ag flakes, which significantly changed with evaporation and removal of solvents and thickeners [32]. Most viscous solvents exhibited low evaporation rates at 140°C , reducing the sinterability between the Ag flakes and ultimately deteriorating the low-temperature processability of the paste. Therefore, in this study, an azeotrope was formed by the optimal combination of two solvent types. Based on the excellent evaporation behavior at 140°C with the azeotrope formations, rapid sintering between the Ag flakes was induced to form a film with excellent electrical conductivity.

2. Materials and Methods

2.1. Ingredients for Paste

Ag flakes (327077-50G, 99.9%, Sigma-Aldrich Co., Ltd., St. Louis, MO, USA) were used as the fillers, and paste formulation included α -terpineol (97%, Daejung Chemicals & Metals Co., Ltd., Siheung, Republic of Korea) as the main viscous solvent. Dipropylene glycol monomethylether (DPMA, 99%, Thermo Fisher Scientific Inc., Waltham, MA, USA) and diethylene glycol dimethyl ether (DGDE, 99%, Thermo Fisher Scientific Inc.) were used as azeotrope-forming solvents, and hydroxypropyl cellulose (HPC; H0474, Tokyo Chemical Industry Co., Ltd., Tokyo, Japan) was used as both a thickener and a thixotropy agent. The role of the thickener is to increase viscosity with a minimal amount, contributing to the stable formation of electrode patterns. The organic ingredients were summarized in Table 1.

Table 1. Chemical and physical properties of viscous solvents and powders used in the paste preparation.

Solvent	Molecular Formular	Chemical Structure	Molecular Weight (g/mol)	Melting Point ($^\circ\text{C}$)	Boiling Point ($^\circ\text{C}$)	Decomposition Temp. ($^\circ\text{C}$)	Viscosity (mPa·s at 20°C)
α -Terpineol	$\text{C}_{10}\text{H}_{18}\text{O}$		154.25	31	210	-	20
DPMA	$\text{C}_{10}\text{H}_{18}\text{O}_3$		190.23	-23	216	-	4.5
DGDE	$\text{C}_6\text{H}_{14}\text{O}_4$		162.23	-64	190	-	0.95
HPC	$(\text{C}_6\text{H}_{10}\text{O}_5)_n$ $[(\text{OC}_3\text{H}_6\text{OH})(\text{OH})_3]_{n-3}$		100,000	-	-	130–200	6–10 (2% aqueous solution)

2.2. Paste Preparation and Sintering

The mixed azeotropic solvents were prepared by placing the solvents in a glass bottle at specific ratios and mixing at 2000 rpm for 10 min using a vortex mixer (VM-96M, Jeiotech, Daejeon, Republic of Korea). For the thixotropic formulations, an appropriate HPC amount was added and mixed for an additional hour to prepare the final mixed solvent. Subsequently, the Ag flakes were mixed with the mixed solvents at a weight ratio of 85:15 to prepare a paste. The prepared paste was printed on a glass slide using a stencil mask with a slit volume of $5.0 \text{ mm} \times 5.0 \text{ mm} \times 0.1 \text{ mm}$. The printed films were sintered in a furnace at 140°C for 10–30 min in air. The average heating rate was $50^\circ\text{C}/\text{min}$ to the

temperature of 140 °C. The sintering time was calculated from the insertion point of the sample when the furnace temperature reached 140 °C. After sintering, the samples were removed from the furnace and cooled in air.

2.3. Characterization

The particle sizes of the Ag flakes were measured using a laser particle size analyzer (PSA, LS I3 320, Beckman counter, Brea, CA, USA), and the d_{50} values and average sizes were calculated. The evaporation behavior of the solvents was analyzed through weight measurements using a moisture analyzer (WBA-110M, Daihan Scientific Co., Ltd., Wonju, Republic of Korea). Specifically, 3 g of solvent was placed on the plate of the moisture analyzer and heated to 140 °C. The weight change over time was monitored until the solvent was completely evaporated. The morphologies of the Ag flakes and microstructures of the sintered films after heat treatment were observed using high-resolution field-emission scanning electron microscopy (HR-FE-SEM, SU8010, Hitachi, Tokyo, Japan). Additionally, the amount of residual HPC in the sintered films was confirmed by a carbon content analysis using energy-dispersive X-ray spectroscopy (EDS, Noran System 7, Thermo Fisher Scientific Inc., Waltham, MA, USA). The thermal behaviors of the prepared pastes were confirmed using thermogravimetry differential thermal analysis (TG-DTA, DTG-60, Shimadzu, Kyoto, Japan) by heating to 140 °C at a rate of 10 °C/min and maintaining the temperature for 60 min. The electrical properties of the sintered films were evaluated by electrical resistance measurements ten times using a four-point probe connected to a source meter (2400, Keithley, Cleveland, OH, USA). The electrical resistivity was calculated to extract the average value and standard deviation.

3. Results and Discussion

Figure 1 shows the SEM images of the Ag flakes, with the average size of 5.60 μm and agglomeration, primarily around smaller flakes. Figure 2 shows the particle-size distribution with the measured d_{10} , d_{50} , and d_{90} values of 1.79, 4.05, and 10.37 μm , respectively, indicating a bimodal size distribution with flakes in the tens of micrometers range.

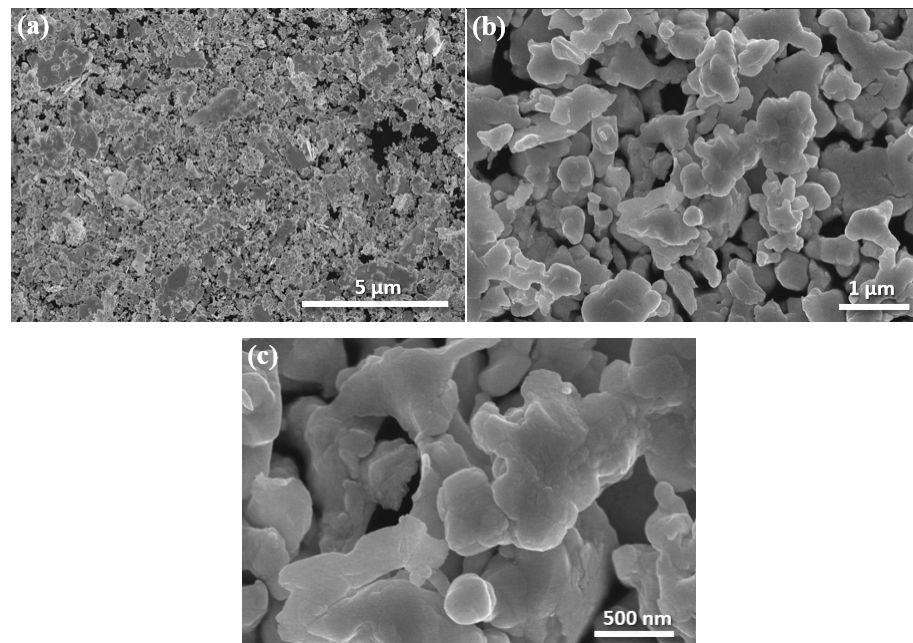
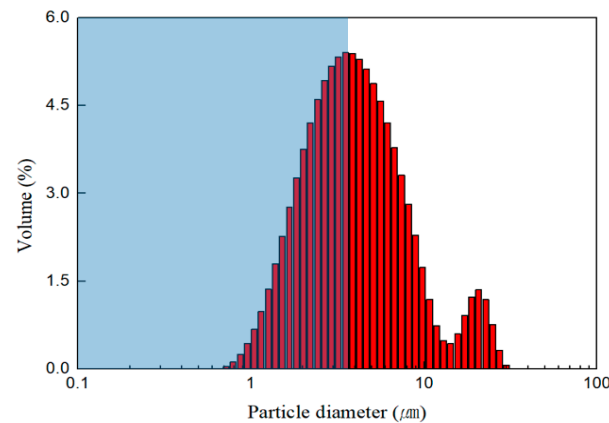


Figure 1. SEM images of the Ag flakes at different magnifications: (a) 2000, (b) 10,000, and (c) 50,000 times.



Size (μm)	Min.	d10	d50	d90	Max.	Mean
	0.60	1.79	4.05	10.37	36.24	5.60

Figure 2. Laser PSA analysis result of the Ag flakes.

Figure 3 shows the evaporation behavior of the main viscous solvent, α -terpineol, and two azeotrope-forming solvents (DPMA and DGDE) at 140 °C over time. All three solvents evaporated completely in 20 min; however, their evaporation rates varied significantly. Specifically, the evaporation rate was as follows: DGDE > DPMA > α -terpineol. This indicates the inverse proportional relationship between the viscosity and evaporation rate.

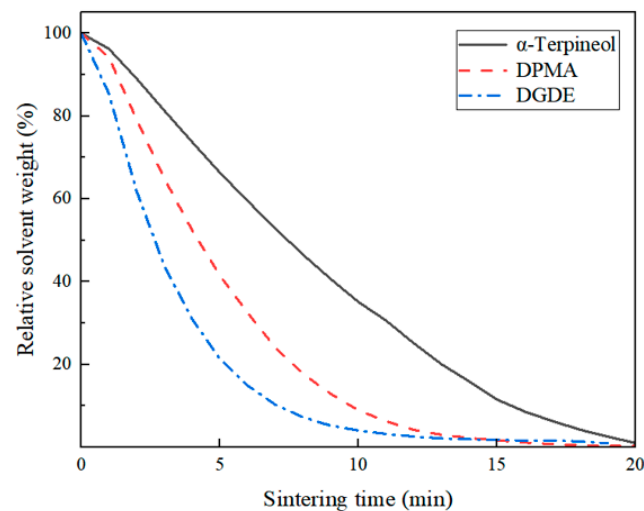


Figure 3. Weight loss of α -terpineol, DPMA, and DGDE over time at 140 °C.

The evaporation behavior changes with the amount of azeotrope-forming solvent added to induce rapid evaporation of α -terpineol, as presented in Figure 4. The most drastic results were obtained when DPMA was mixed with α -terpineol (Figure 4a), with the mixed solvent exhibiting a higher evaporation rate than pure DPMA, achieving the rapid evaporation by azeotrope formation. At a 50:50 weight ratio, evaporation was completed in approximately 11.7 min, with the highest evaporation rate. In contrast, the evaporation rate with DGDE mixed with α -terpineol was between that of pure α -terpineol and pure DPMA when one solvent was in excess (Figure 4b). However, the evaporation rate at a 50:50 mixing ratio is higher than that of pure DGDE, achieving the desired result. Therefore, mixtures of α -terpineol and DPMA and α -terpineol and DGDE at compositions of 50:50 were considered as the basic compositions of the mixed solvent in subsequent studies for

preparing an optimal paste. When DPMA and DGDE were mixed without α -terpineol (Figure 4c), the attempted mixing ratios had a lower evaporation rate than pure DGDE, indicating the absence of azeotrope formation. Based on these results, eight mixed solvent compositions with a small amount of thickener are listed in Table 2. HPC, which was used as a thickener, significantly improved the viscosity and thixotropy of the paste, even with small additions (1, 2, and 3 wt%), leading to significant improvements in the printability of the paste. This is an important factor that significantly affected the sinterability between the Ag flakes and the electrical resistivity of the sintered film.

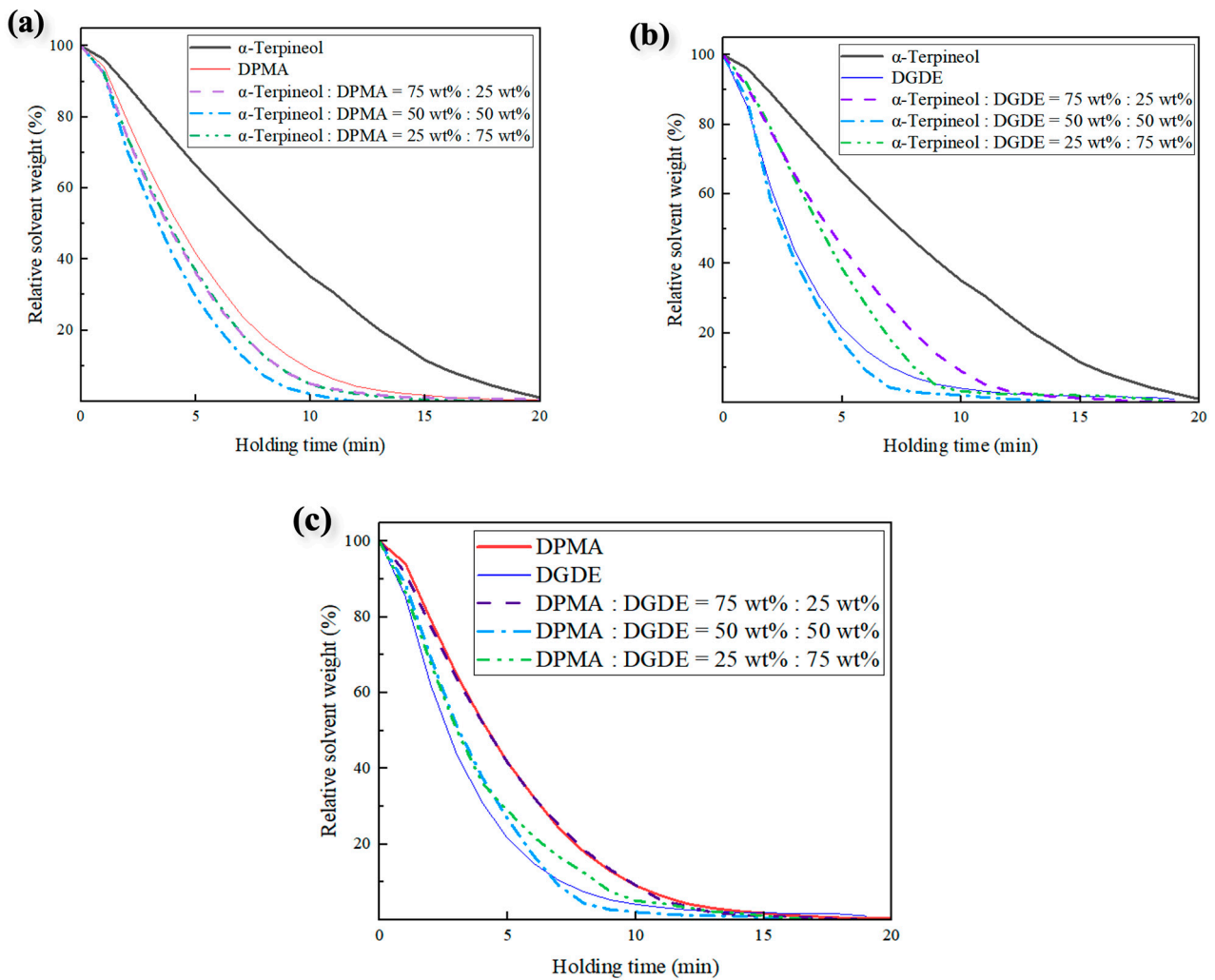


Figure 4. Weight-loss graphs of nine mixed solvents over time at 140 °C: (a) α -terpineol and DPMA, (b) α -terpineol and DGDE, and (c) DPMA and DGDE.

Table 2. Compositions of the investigated solvent mixtures for the paste formulation.

Solvent	Solvent 1	Solvent 2	HPC
#1	α -Terpineol (50 wt%)	DPMA (50 wt%)	0 wt%
#2	α -Terpineol (49.5 wt%)	DPMA (49.5 wt%)	1 wt%
#3	α -Terpineol (49 wt%)	DPMA (49 wt%)	2 wt%
#4	α -Terpineol (48.5 wt%)	DPMA (48.5 wt%)	3 wt%
#5	α -Terpineol (50 wt%)	DGDE (50 wt%)	0 wt%
#6	α -Terpineol (49.5 wt%)	DGDE (49.5 wt%)	1 wt%
#7	α -Terpineol (49 wt%)	DGDE (49 wt%)	2 wt%
#8	α -Terpineol (48.5 wt%)	DGDE (48.5 wt%)	3 wt%

Figure 5 shows the evaporation of the eight mixed solvents, including those with 1–3 wt% HPC thickener at 140 °C over time. In the α -terpineol/DPMA mixed solvents (Figure 5a), the evaporation rate decreased with increasing HPC content. With 1 wt% HPC, the mixed solvents are almost completely evaporated in 12.5 min. Similarly, the evaporation rate in the α -terpineol/DGDE mixed solvents (Figure 5b) decreases with increasing HPC content, whereas that with 1 wt% HPC decreases minimally, completely evaporating the solvent in 8 min. Therefore, under identical processing conditions, compositions with 1 wt% HPC are identified as the most effective for inducing rapid sintering in high-viscosity α -terpineol/DPMA mixed solvents and low-viscosity α -terpineol/DGDE mixed solvents.

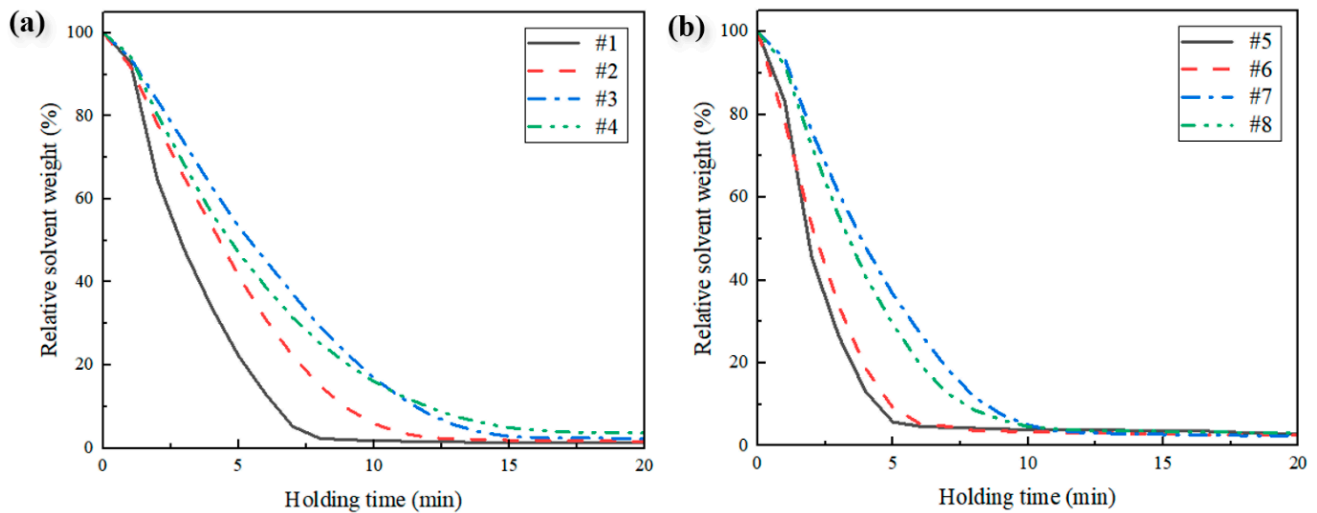


Figure 5. Weight-loss graphs of eight mixed solvents with the HPC thickener over time at 140 °C: (a) α -terpineol/DPMA mixed solvents and (b) α -terpineol/DGDE mixed solvents.

The TG-DTA results of the pastes prepared with various mixed solvents under dynamic and isothermal mixed heating conditions, similar to the actual sintering temperature profile, are shown in Figure 6. In the DPMA-containing specimens (Figure 6a), an endothermic reaction began during the heating onset. Significant weight loss by solvent evaporation is observed at temperatures above 70 °C. Endothermic peaks are observed in the range of 130.0–139.1 °C, and continuous weight loss is observed until reaching 140 °C. However, in the sample with 1 wt% HPC (#2), a small exothermic behavior at 103 °C and a delay in weight loss are observed, which could be attributed to the sintering of Ag flakes. Moreover, the delay in weight loss can be ascribed to the blockage of the outgassing pathways by sintering. Meanwhile, in the DGDE-containing specimens (Figure 6b), weight loss due to solvent evaporation is observed, starting at a notably lower temperature of 40 °C in the sample with 1 wt% HPC (#6), and completing before reaching 140 °C. The endothermic peak ascribed to solvent evaporation is observed at 126.4 °C, which is considerably lower temperature than the other mixed solvents owing to the formation of an azeotrope with an appropriate HPC amount, thereby improving the evaporation behavior and positively affecting the sintering of Ag flakes. For sample #6, a small exothermic peak is observed at approximately 140 °C after solvent evaporation, which can be ascribed to the sintering of Ag flakes.

The printability of the eight pastes is shown in Figure 7. For the pastes without HPC (#1 and #5), the low viscosity and thixotropy collapsed the printed patterns. However, these issues are mitigated as the HPC content is increased. In particular, in the DPMA-containing pastes, which were predicted to have higher viscosity, excellent printability with almost no pattern collapse is observed in the composition with 2 wt% HPC. Except for #1 and #5, the average thickness of the printed patterns was measured to be 92.5 (\pm 2.1) μ m.

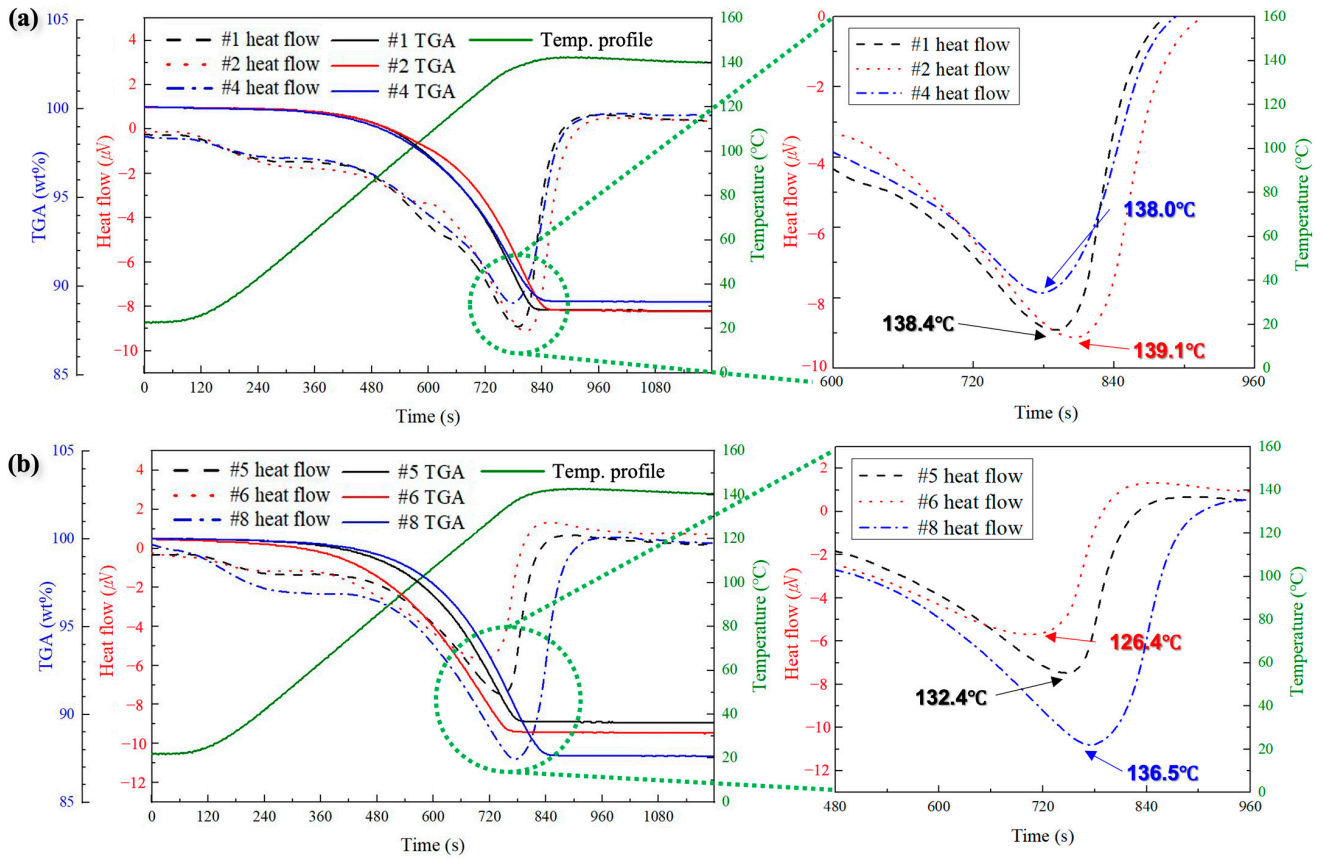


Figure 6. TG-DTA curves of the Ag pastes with (a) α -terpineol/DPMA(/HPC) and (b) DGDE/ α -Terpineol(/HPC) mixtures.

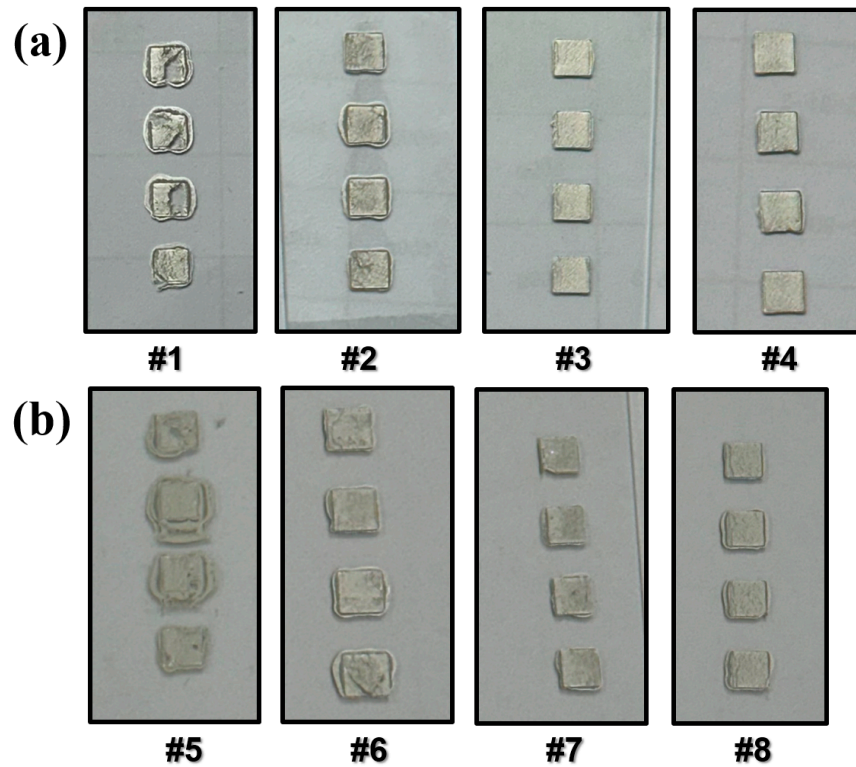


Figure 7. Images of screen-printed films using Ag pastes prepared with different mixed solvents and HPC contents: (a) α -terpineol/DPMA(/HPC) and (b) DGDE/ α -Terpineol(/HPC) mixtures.

Figure 8 shows the electrical resistivities and sheet resistances of films from the printed patterns after sintering at 140 °C with respect to the Ag paste type and sintering time. For the specimens containing DPMA (Figure 8a), the resistivity of the pastes gradually decreases with increasing sintering time. Compared to the paste without HPC (#1), HPC addition significantly decreased the resistivity after sintering for 20 min. After sintering for 30 min, the resistivity greatly decreased for pastes #1 and #2, whereas a minimal decrease is observed in pastes #3 and #4, which had a higher HPC content. Consequently, paste #2 with 1 wt% HPC has the lowest resistivity of $7.72 \times 10^{-6} \Omega \cdot \text{cm}$ obtained in 30 min at 140 °C. Therefore, when compared to previous similar results [14–26], the achieved resistivity is evaluated as an excellent value. This suggests that HPC addition improved the contact between the Ag flakes owing to the improved printability, providing positive results after up to 20 min of sintering. However, in pastes #3 and #4 with higher HPC contents, the residual HPC is expected to limit the sintering of the flakes after 20 min of sintering. In contrast, paste #2 with an appropriate HPC amount continued to exhibit excellent sinterability owing to improved contact between Ag flakes without the hindrance of residual HPC, as observed from the exothermic results obtained starting at 103 °C in Figure 6a.

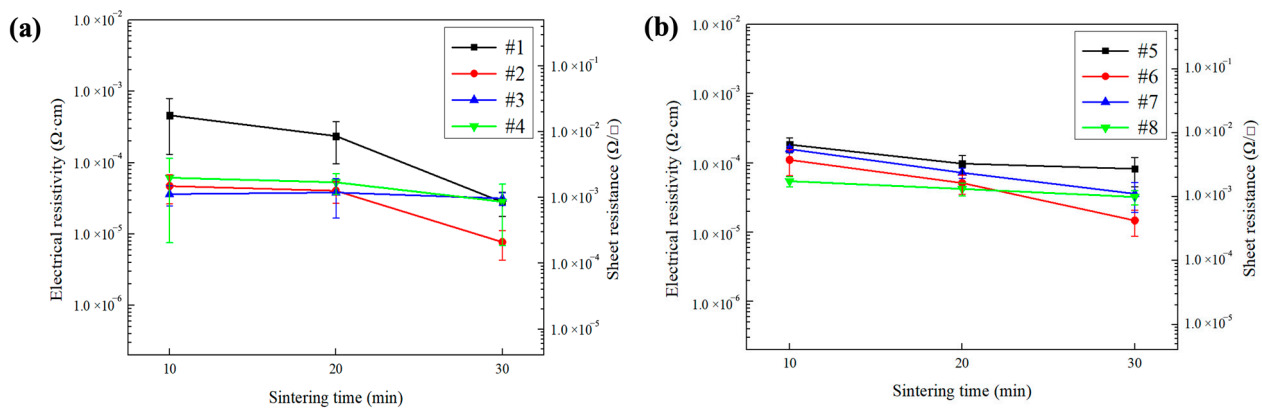


Figure 8. Electrical resistivities and sheet resistances of the films sintered at 140 °C with different HPC contents and sintering times: (a) α -terpineol/DPMA mixed solvents and (b) α -terpineol/DGDE mixed solvents.

For the specimens with DGDE (Figure 8b), paste #5 inherently provides a lower resistivity, which can be considered an early sintering start effect by previously observed high evaporation rates. All pastes exhibit a gradual decrease in resistivity with increasing sintering time, and the HPC addition tends to decrease the resistivity. However, minimal resistivity reduction due to HPC addition is noted owing to its inherently low viscosity. Similarly, paste #6 with 1 wt% HPC has a low resistivity of $1.47 \times 10^{-5} \Omega \cdot \text{cm}$ after sintering for 30 min.

The HPC is an organic compound including C; thus, the residual HPC amount in the sintered film can be compared by the C content. The C content in the film maintained for 30 min was measured by EDS to confirm that the residual amount in the sintered film increases with the HPC content during heating at 140 °C. The results are shown in Figure 9. The measured C content increased with the HPC content in the specimens with DPMA and DGDE, indicating that the initial HPC content in the paste is proportional to the residual HPC content in the sintered film at 140 °C. Therefore, the insufficient resistance values observed in the pastes containing 2 or 3 wt% HPC after 30 min of sintering are attributed to the residual HPC content.

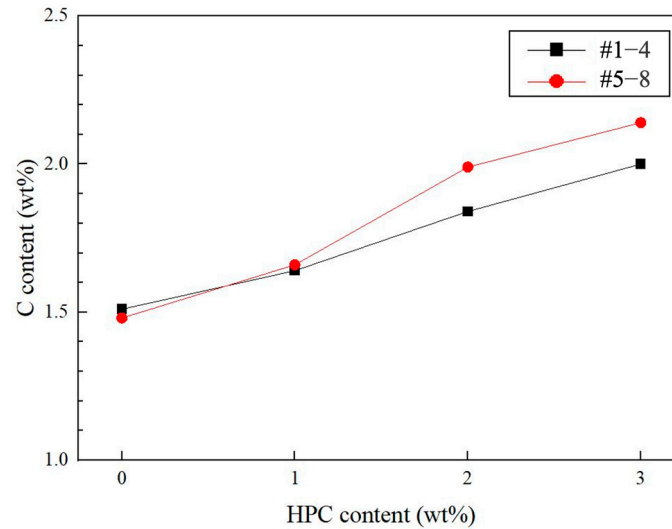


Figure 9. C contents measured in the films based on paste samples with different HPC contents after sintering for 30 min at 140 °C in air, as obtained by EDS.

Figure 10 shows the surface microstructures of the films formed by the pastes with DPMA and varying HPC contents and sintering times at 140 °C. The microstructure of the film sintered for 30 min using paste #2 has the widest sintered area and best connectivity between the flakes compared to the microstructures under all other conditions (note the larger grain indicated by the arrow). Such microstructure corresponds well to the lowest electrical resistivity ($7.72 \times 10^{-6} \Omega \cdot \text{cm}$) measured for the paste #2 after 30 min of sintering, as shown in Figure 8a. Figure 11 also shows that paste #6 sintered for 30 min exhibits the largest sintered area with well-established interconnections between the flakes compared with pastes #5, #7, and #8.

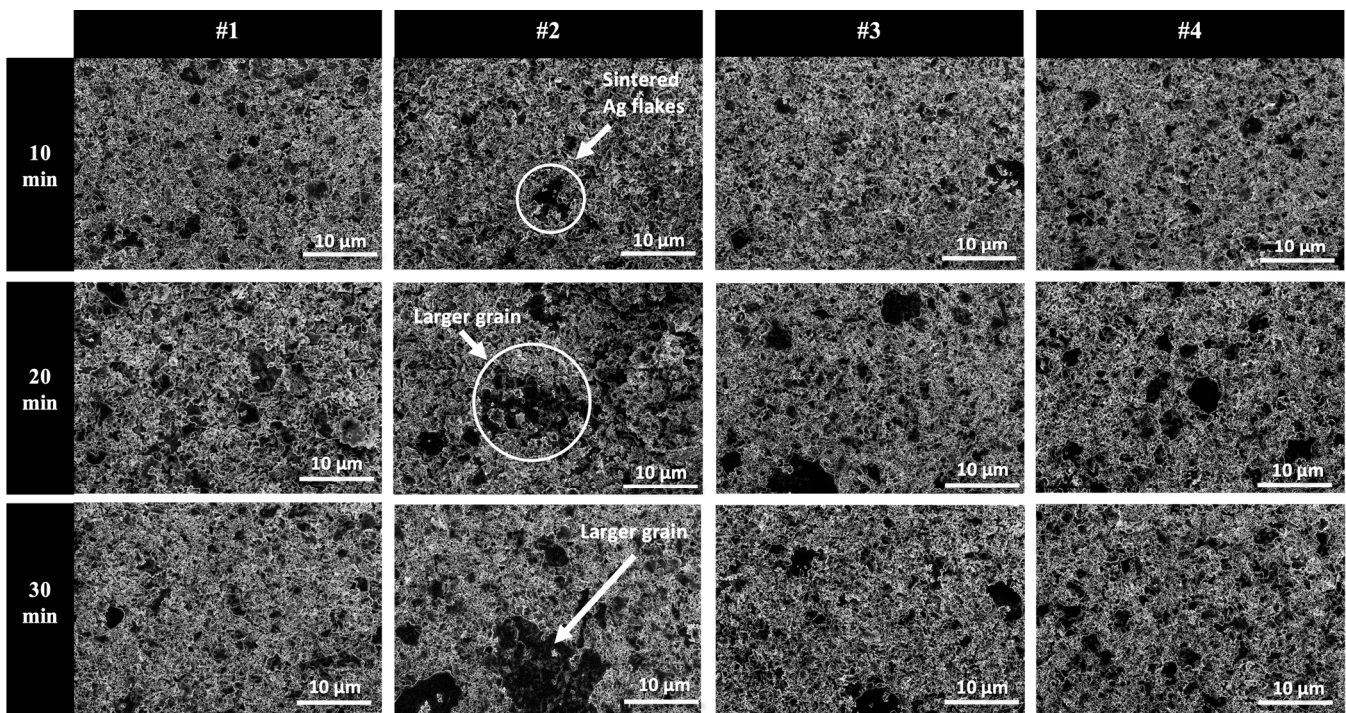


Figure 10. Surface SEM images of the films sintered at 140 °C in air using α -terpineol/DPMA-based pastes with different HPC contents and sintering times.

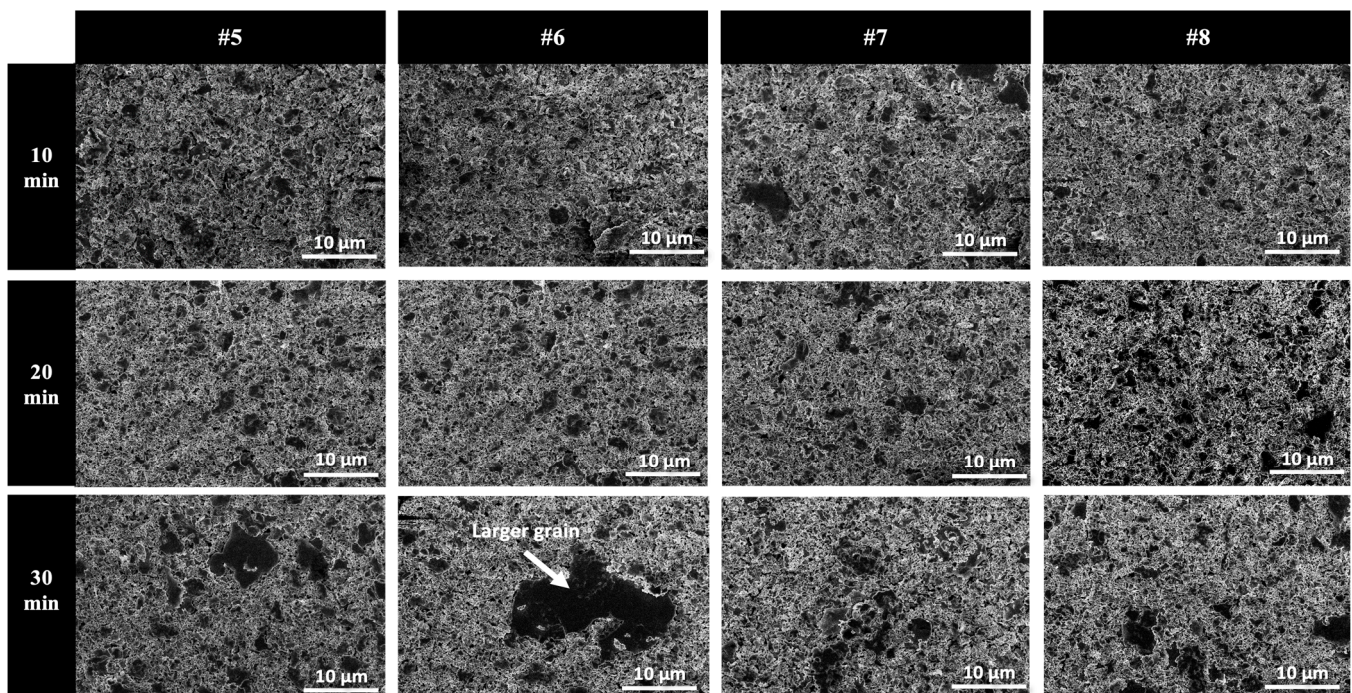


Figure 11. Surface SEM images of the films sintered at 140 °C in air using α -terpineol/DGDE-based pastes with different HPC contents and sintering times.

4. Conclusions

A resin-free low-temperature evaporative solvent-based paste formulation was implemented to form a film with low electrical resistivity through rapid sintering between micron-sized Ag flakes at a low temperature of 140 °C. Specifically, α -terpineol was used as the main viscous solvent, with DGDE or DPMA added as the azeotrope-forming solvents to greatly improve the evaporation rate. Finally, an HPC thickener was added to increase the viscosity and thixotropy. The paste containing 49.5 wt% α -terpineol, 49.5 wt% DPMA, and 1 wt% HPC exhibited improved contacts between the Ag flakes and overall percolation connectivity due to its good printability and early sintering owing to the improved evaporation behavior, resulting in a rapid decrease in the electrical resistivity even at 140 °C. Specifically, the film using this paste and sintered for 30 min exhibited the lowest resistivity of $7.72 \times 10^{-6} \Omega\cdot\text{cm}$, with the early exothermic behavior starting at 103 °C owing to sintering. The microstructure of the formed film exhibited the widest sintered area and best connectivity between flakes. Although increasing the HPC content to 3 or 4 wt% further improved the printability, the resistivity values slightly increased after sintering for 30 min owing to the increased residual HPC. The paste with 49.5 wt% α -terpineol, 49.5 wt% DGDE, and 1 wt% HPC demonstrated reduced printability due to the decreased viscosity, whereas the maximum evaporation rate obtained with 1 wt% HPC resulted in the highest resistivity of $1.47 \times 10^{-5} \Omega\cdot\text{cm}$ after sintering for 30 min.

Author Contributions: Conceptualization, J.-H.L.; methodology, S.H.J. and J.-H.L.; validation, S.H.J. and J.E.P.; formal analysis, S.H.J., J.E.P. and J.-H.L.; investigation, S.H.J., J.E.P. and J.-H.L.; resources, J.-H.L.; data curation, S.H.J. and J.E.P.; writing—original draft preparation, S.H.J. and J.-H.L.; writing—review and editing, J.-H.L.; visualization, S.H.J. and J.E.P.; supervision, J.-H.L.; project administration, J.-H.L.; funding acquisition, J.-H.L. All authors have read and agreed to the published version of the manuscript.

Funding: This study was supported by Korea Electric Power Corporation. (Grant number: R23XO05-02).

Data Availability Statement: The original contributions presented in the study are included in the article, further inquiries can be directed to the corresponding author.

Conflicts of Interest: The authors declare no conflicts of interest. The funders had no role in the design of the study, in the collection, analyses, or interpretation of data, in the writing of the manuscript, or in the decision to publish the results.

References

1. Gao, L.; Chao, L.; Hou, M.; Liang, J.; Chen, Y.; Yu, H.; Huang, W. Flexible, transparent nanocellulose paper-based perovskite solar cells. *npj Flex. Electron.* **2019**, *3*, 1–8. [[CrossRef](#)]
2. Lee, K.-T.; Jang, J.-Y.; Park, S.J.; Ok, S.A.; Park, H.J. Incident-angle-controlled semitransparent colored perovskite solar cells with improved efficiency exploiting a multilayer dielectric mirror. *Nanoscale* **2017**, *9*, 13983–13989. [[CrossRef](#)] [[PubMed](#)]
3. Cui, D.; Yang, Z.; Yang, D.; Ren, X.; Liu, Y.; Wei, Q.; Fan, H.; Zeng, J.; Liu, S. Color-tuned perovskite films prepared for efficient solar cell applications. *J. Phys. Chem. C* **2016**, *120*, 42–47. [[CrossRef](#)]
4. Schlisske, S.; Mathies, F.; Busko, D.; Strobel, N.; Rödlmeier, T.; Richards, B.; Lemmer, U.; Paetzold, U.; Hernández-Sosa, G.; Klampaftis, E. Design and color flexibility for inkjet-printed perovskite photovoltaics. *ACS Appl. Energy Mater.* **2019**, *2*, 764–769. [[CrossRef](#)]
5. Quiroz, C.O.R.; Bronnbauer, C.; Levchuk, I.; Hou, Y.; Brabec, C.J.; Forberich, K. Coloring semitransparent perovskite solar cells via dielectric mirrors. *ACS Nano* **2016**, *10*, 5104–5112. [[CrossRef](#)]
6. Bati, A.S.R.; Zhong, Y.L.; Burn, P.L.; Nazeeruddin, M.K.; Shaw, P.E.; Batmunkh, M. Next-generation applications for integrated perovskite solar cells. *Commun. Mater.* **2023**, *4*, 2. [[CrossRef](#)]
7. Bing, J.; Granados Caro, L.; Talathi, H.P.; Chang, N.L.; McKenzie, D.R.; Ho-Baillie, A.W.Y. Perovskite solar cells for building integrated photovoltaics—Glazing applications. *Joule* **2022**, *6*, 1446–1474. [[CrossRef](#)]
8. Zhu, Y.; Shu, L.; Fan, Z. Recent Progress on Semi-transparent Perovskite Solar Cell for Building-integrated Photovoltaics. *Chem. Res. Chin. Univ.* **2020**, *36*, 366–376. [[CrossRef](#)]
9. Koh, T.M.; Wang, H.; Ng, Y.F.; Bruno, A.; Mhaisalkar, S.; Mathews, N. Halide Perovskite Solar Cells for Building Integrated Photovoltaics: Transforming Building Façades into Power Generators. *Adv. Mater.* **2022**, *34*, 2104661. [[CrossRef](#)]
10. Wang, H.; Li, J.; Dewi, H.A.; Mathews, N.; Mhaisalkar, S.; Bruno, A. Colorful Perovskite Solar Cells: Progress, Strategies, and Potentials. *J. Phys. Chem. Lett.* **2021**, *12*, 1321–1329. [[CrossRef](#)]
11. Mujahid, M.; Chen, C.; Zhang, J.; Li, C.; Duan, Y. Recent advances in semitransparent perovskite solar cells. *InfoMat* **2021**, *3*, 101–124. [[CrossRef](#)]
12. Nazir, G.; Lee, S.-Y.; Lee, J.-H.; Rehman, A.; Lee, J.-K.; Seok, S.I.; Park, S.-J. Stabilization of Perovskite Solar Cells: Recent Developments and Future Perspectives. *Adv. Mater.* **2022**, *34*, 2204380. [[CrossRef](#)] [[PubMed](#)]
13. Rakocevic, L.; Gehlhaar, R.; Jaysankar, M.; Song, W.; Aernouts, T.; Fledderus, H.; Poortmans, J. Translucent, color-neutral and efficient perovskite thin film solar modules. *J. Mater. Chem. C* **2018**, *6*, 3034–3041. [[CrossRef](#)]
14. Yang, D.; Huang, Y.; Tian, Y. Microstructure of Ag nano paste joint and its influence on reliability. *Crystals* **2021**, *11*, 1537. [[CrossRef](#)]
15. Yang, H. Study on the preparation process and sintering performance of doped nano-silver paste. *Rev. Adv. Mater. Sci.* **2022**, *61*, 969–976. [[CrossRef](#)]
16. Ma, L.; Wang, Y.; Jia, Q.; Zhang, H.; Wang, Y.; Li, D.; Zou, G.; Guo, F. Low-temperature-sintered nano-Ag film for power electronics packaging. *J. Electron. Mater.* **2024**, *53*, 228–237. [[CrossRef](#)]
17. Chen, C.; Choe, C.; Kim, D.; Zhang, Z.; Long, X.; Zhou, Z.; Wu, F.; Suganuma, K. Effect of oxygen on microstructural coarsening behaviors and mechanical properties of Ag sinter paste during high-temperature storage from macro to micro. *J. Alloys Compd.* **2020**, *834*, 155173. [[CrossRef](#)]
18. Yan, J. A Review of Sintering-Bonding Technology Using Ag Nanoparticles for Electronic Packaging. *Nanomaterials* **2021**, *11*, 927. [[CrossRef](#)]
19. Divitini, G.; Cacovich, S.; Matteocci, F.; Cinà, L.; Di Carlo, A.; Ducati, C. In situ observation of heat-induced degradation of perovskite solar cells. *Nat. Energy* **2016**, *1*, 15012. [[CrossRef](#)]
20. Sasaki, K.; Mizumura, N. Development of Low-temperature Sintering Nano-Ag Pastes Using Lowering Modulus Technologies. In Proceedings of the IEEE 17th International Conference on Nanotechnology (IEEE-NANO), Pittsburgh, PA, USA, 25–28 July 2017.
21. Jung, K.-H.; Min, K.D.; Lee, C.-J.; Park, B.-G.; Jung, H.; Koo, J.-M.; Lee, B.; Jung, S.-B. Effect of epoxy content in Ag nanoparticle paste on the bonding strength of MLCC packages. *Appl. Surf. Sci.* **2019**, *495*, 143487. [[CrossRef](#)]
22. Ho, L.N.; Wu, T.F.; Nishikawa, H. Properties of Phenolic-Based Ag-Filled Conductive Adhesive Affected by Different Coupling Agents. *J. Adhes.* **2013**, *89*, 847–858. [[CrossRef](#)]
23. Wu, H.; Chiang, S.; Han, W.; Tang, Y.; Kang, F.; Yang, C. Surface iodination: A simple and efficient protocol to improve the isotropically thermal conductivity of silver-epoxy pastes. *Compos. Sci. Technol.* **2014**, *99*, 109–116. [[CrossRef](#)]
24. Fang, S.; Zhang, Y.; Huang, C.; Liu, P.; Zhang, C.; Liu, Y.; Li, S. Hybrid silver pastes with synergistic effect of multi-scale silver fillers and the application in flexible circuits. *J. Mater. Sci. Mater. Electron.* **2021**, *32*, 13777–13786. [[CrossRef](#)]
25. Zhao, L.; Lin, Z.; Liu, Y.; Shi, Z.; Yu, L.; Li, Z. Parametric study on conductive patterns by low-temperature sintering of micron silver ink. *J. Mater. Sci. Mater. Electron.* **2023**, *34*, 653–659. [[CrossRef](#)]

26. Liu, X.; Wu, S.; Chen, B.; Ma, Y.; Huang, Y.; Tang, S.; Liu, W. Tuning the electrical resistivity of conductive silver paste prepared by blending multi-morphologies and micro-nanometers silver powder. *J. Mater. Sci. Mater. Electron.* **2021**, *32*, 13777–13786. [[CrossRef](#)]
27. Noh, S.; Choe, C.; Chen, C.; Zhang, H.; Suganuma, K. Printed wire interconnection using Ag sinter paste for wide band gap power semiconductors. *J. Mater. Sci. Mater. Electron.* **2018**, *29*, 15223–15232. [[CrossRef](#)]
28. Zhang, H.; Nagao, S.; Suganuma, K.; Albrecht, H.-J.; Wilke, K. Thermostable Ag die-attach structure for high-temperature power devices. *J. Mater. Sci. Mater. Electron.* **2016**, *27*, 1337–1345. [[CrossRef](#)]
29. Yang, F.; Hu, B.; Peng, Y.; Hang, C.; Chen, H.; Lee, C.; Wei, J.; Li, M. Ag microflake-reinforced nano-Ag paste with high mechanical reliability for high-temperature applications. *J. Mater. Sci. Mater. Electron.* **2019**, *30*, 5526–5532. [[CrossRef](#)]
30. Martin, H.A.; Hu, D.; Liu, X.; Poelma, R.H.; Smits, E.C.P.; Van Driel, W.D.; Zhang, G. Prognostic Monitoring of Power QFN Packages with Silver Sintered Die-Attach Materials. *IEEE Trans. Compon. Packag. Manuf. Technol.* **2024**. [[CrossRef](#)]
31. Wang, M.; Mei, Y.-H.; Jin, J.; Chen, S.; Li, X.; Lu, G.-Q. Pressureless Sintered-Silver Die-Attach at 180 °C for Power Electronics Packaging. *IEEE Trans. Power Electron.* **2021**, *36*, 12141–12145. [[CrossRef](#)]
32. Yao, S.; Xing, J.; Zhang, J.; Xiong, S.; Yang, Y.; Yuan, X.; Li, H.; Tong, H. Microscopic investigation on sintering mechanism of electronic silver paste and its effect on electrical conductivity of sintered electrodes. *J. Mater. Sci. Mater. Electron.* **2018**, *29*, 18540–18546. [[CrossRef](#)]

Disclaimer/Publisher’s Note: The statements, opinions and data contained in all publications are solely those of the individual author(s) and contributor(s) and not of MDPI and/or the editor(s). MDPI and/or the editor(s) disclaim responsibility for any injury to people or property resulting from any ideas, methods, instructions or products referred to in the content.